Tertiary Amine Based Amino-yne Click Polymerization toward Multifunctional Poly(β-ammonium acrylate)s

Xinyu Xu[a,b], *Jie Chen*[a,b], *Anjun Qin*[a,b,]*, *and Ben Zhong Tang*[b,c,d]

[a] State Key Laboratory of Luminescent Materials and Devices, Guangdong Provincial Key Laboratory of Luminescence from Molecular Aggregates, South China University of Technology, Guangzhou 510640, China

[b] Center for Aggregation-Induced Emission, AIE Institute, South China University of Technology, Guangzhou 510640, China

[c] School of Science and Engineering, Shenzhen Institute of Aggregate Science and Technology, The Chinese University of Hong Kong, Shenzhen (CUHK-Shenzhen), Guangdong 518172, China

[d] Hong Kong Branch of Chinese National Engineering Research Centre for Tissue Restoration and Reconstruction, The Hong Kong University of Science & Technology, Clear Water Bay, Kowloon, Hong Kong 999077, China.

* Corresponding author: msqinaj@scut.edu.cn

ABSTRACT: Polyelectrolytes possess many unique properties because of their charged groups, which have been widely utilized in the construction of functional materials. However, the synthesis of polyelectrolytes was often carried out under harsh conditions such as high temperature or precious metal catalyst. In this work, we innovatively proposed tertiary amine self-initiation strategy to realize the click reaction of activated alkynes, tertiary amines and protic acids. Accordingly, tertiary amine-based amino-yne click polymerization was successfully established and a series of main-chain charged polyelectrolytes were efficiently prepared under ambient conditions. The resultant poly(β-ammonium acrylate)s (PAAs) exhibit ionic cluster luminescence and it can be easily regulated through altering anions. Furthermore, we utilized thiophenol compounds achieving the degradation and reconstruction of PAAs. The refractive indices of reconstructed polymers have been greatly improved (Δn = 0.2). Through tertiary amine-based amino-yne click polymerization in this work, amino acid was easily introduced into the polymers. The resultant polyelectrolyte shows astonishing adhesive ability for various substrates. The adhesive strength and work of debonding for stainless steel can reach 6.4 MPa and 14315 Nm^{-1}, respectively. These results demonstrate the high efficiency of tertiary amine-based amino-yne click reactions and the tunability of polymer structures, which indicates the infinite potential for the preparation and application of multifunctional PAA.

INTRODUCTION

Polyelectrolytes are widely present in nature. Natural polyelectrolytes, such as DNA and proteins, many of which are the material basis for the continuation and activity of life.[1-5] Polyelectrolytes possess many properties that differ from traditional polymers due to their charged groups. Recently, more and more synthesized functional polyelectrolytes have been reported. Structurally, polyelectrolytes can be divided into conjugated and non-conjugated polyelectrolytes. Conjugated polyelectrolytes are commonly used in capacitors, solar cells, optoelectronic devices, etc.[6-10] Non-conjugated polyelectrolytes are mainly applied in fields such as water treatment, ionic conductors, artificial muscles, soft actuators, etc.[11-17] According to the position of charged groups, polyelectrolytes can be further divided into side-chain and main-chain charged polyelectrolytes. They can all be synthesized by polymerizing charged monomers or modifying polymer with ionic groups after polymerization.[18-22]

However, the synthesis of main-chain charged polyelectrolytes is more difficult. In recent years, there are few reports on the preparation of main-chain charged polyelectrolytes, mainly due to limited reaction types, harsh conditions, and low reaction efficiency. For instance, Liu et al. synthesized ionized azaquinodiethane monomer, and then prepared quinoidal aromatic conjugated polyelectrolytes via palladium-catalyzed polycoupling.[23] Han et al. synthesized polyelectrolytes by the polymerization of imidazole salts and aromatic alkyne monomers in the presence of rhodium catalysis at 100 ℃ in 24 h.[24] He et al. achieved the polymerization of pyridinium salts and ester-activated alkynes at 60 ℃ in 24 h,[25] and the resultant Poly(*β*-pyridinium acrylate)s possessed good antibacterial activity. This polymerization was conducted without catalyst in air atmosphere, greatly simplifying the experimental operation. However, this polymerization was still not efficient enough, and the resultant polymers don't exhibit stereoselectivity and contain both *E*/*Z* configurations. Therefore, it is highly demand to develop a more efficient one-step method to synthesize main-chain charged polyelectrolytes under milder conditions.

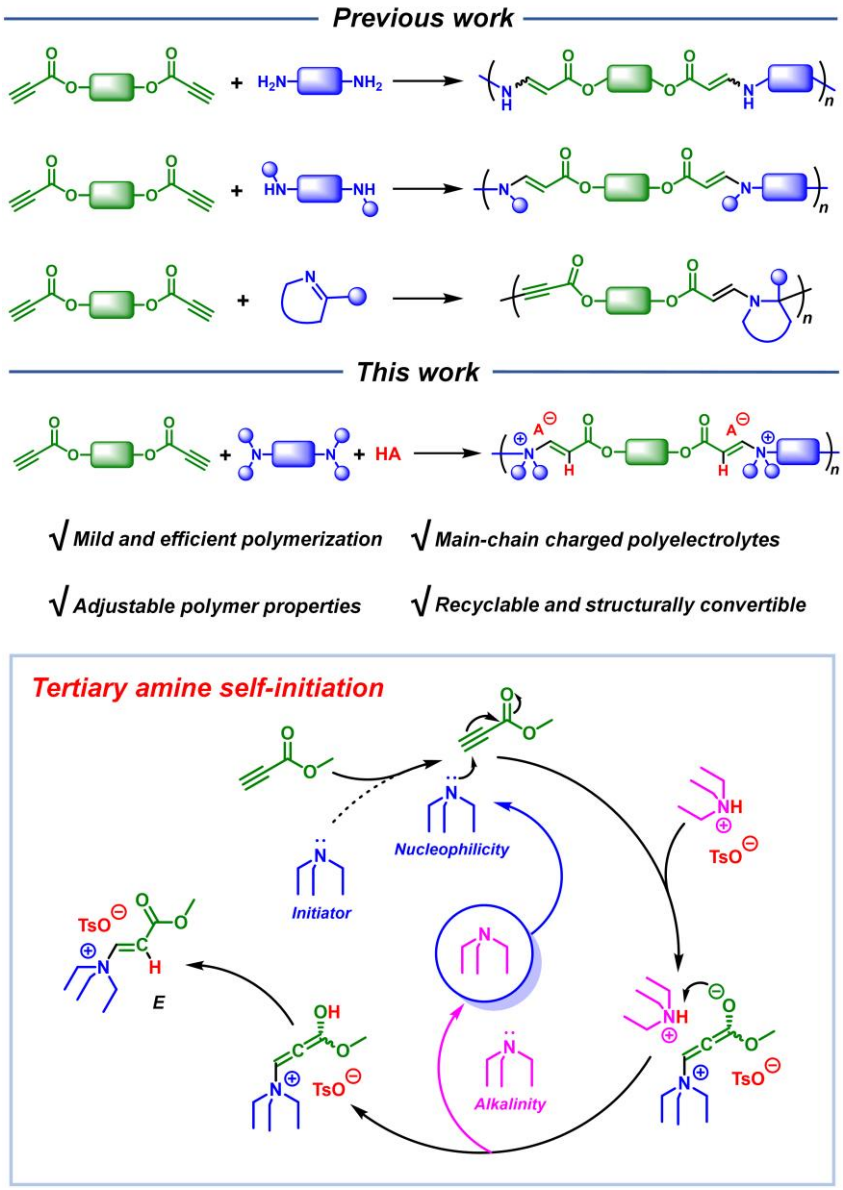

Scheme 1. Tertiary amine self-initiated click reactions of tertiary amines and activated alkynes in the presence of protic acids.

Since Sharpless et al. first proposed the concept of click chemistry in 2001,[26] the family of click reactions is becoming larger and more active. Utilizing click reactions with good atomic economy and high reaction efficiency can make organic synthesis cushier and more convenient. Recently, our group has developed a series of activated alkyne-based click polymerizations.[27] These click polymerizations have the superiorities of mild conditions, high yields, and excellent regio- and stereoselectivity, which have been widely used in diverse areas.[28-33] Activated ethynyl groups own

higher reactivity compared to normal ones, because ethynyl group is connected to electron-withdrawing group increasing the electrophilicity of ethynyl carbon. According to this characteristic, our group has developed click polymerizations of activated alkyne with various nucleophilic groups, such as amino, thiol, hydroxyl ones. The amino-yne click polymerization is the most efficient one, and the polymers can be prepared in high yields under ambient conditions.[34-36] However, the current reports of amine monomers polymerized with activated alkynes only focused on primary amines, secondary amines and imines (Scheme 1),[37] and there are still no reports on tertiary amines. Theoretically, tertiary amines possess nucleophilicity and can react with activated alkynes. However, because tertiary amines could catalyze the self-addition of activated alkynes,[38] it is difficult to realize click reactions between them and activated alkynes.

Aiming to develop tertiary amine-based click polymerizations, we proposed a strategy of tertiary amine self-initiation to solve the problem that they cannot react with each other. This strategy reconstructed the reaction mechanism between tertiary amines and activated alkynes, which prevented tertiary amines catalyzing the activated alkynes self-addition under the synergistic effect of strong protic acid (Scheme 1). Consequently, the tertiary amines could efficiently react with the activated alkynes to generate β-ammonium acrylates (AAs) under mild conditions. Encouraged by this model reaction, we further optimized polymerization conditions and successfully developed an efficient click polymerization of diynes, tertiary amine monomers and protic acids. A series of main-chain charged Poly(β-ammonium acrylate)s (PAAs) were prepared in high yields under ambient conditions. This polymerization provided an efficient and convenient method for the synthesis of polyelectrolytes. The produced polymers exhibited a nontraditional ionic clusteroluminescence due to their charged structures. Afterwards, benefiting from the structure of AAs, we can achieve the precise degradation of polyelectrolytes by nucleophilic substitution of tertiary amine with thiophenol. In this process, the tertiary amines and protic acids can be recovered in high yields, realizing the degradation cycle of PAA. Inspired by degradation property, we used thiophenol monomers to accomplish the backbone reconstruction of polyelectrolytes. The introduction of phenyl sulfide structure greatly improved the refractive index of the polymer (Δn

= 0.2). Finally, amino acid-rich polymer networks were facilely prepared through this powerful amino-yne click polymerization. The resultant polyelectrolytes exhibited excellent adhesive ability to different substrates such as stainless steel, brass, aluminum, and glass.

RESULTS AND DISCUSSIONS

Click reactions of Activated Alkynes, Tertiary Amines and Protic Acids. 1,4-Diazobicyclo[2.2.2]octane (DABCO) can efficiently catalyze the self-addition of activated alkynes because the latter displays a dual role of nucleophilicity and electrophilicity.[38] As DABCO nucleophilically attacks activated ethynyl group, unstable negative intermediate will be formed, which will grab the protons in the reaction system (Scheme S1). In the process of activated alkynes self-addition, the terminal ethynyl groups lose protons, then the generated ethynyl anions will exhibit nucleophilicity, substituting DABCO to complete the self-addition of activated ethynyl groups. This means that if the reaction system only contains tertiary amines and activated alkynes, the former merely serves as a catalyst to facilitating the self-addition of the latter. Therefore, to realize the click reaction of tertiary amines and activated alkynes, it is crucial to introduce other more reactive proton sources to suppress activated alkynes self-addition. More importantly, the anions formed by protic reagents after providing protons must have no nucleophilicity. Otherwise, anions will substitute the tertiary amines to generate side products (Scheme S1). For example, hydroxyl or thiol groups will provide protons and complete the alkoxylation or thiohydrogenation of activated alkynes.[39-42]

Based on above analysis, we speculate that utilizing strong protic acids will realize the click reaction of tertiary amines and activated alkynes, because the anions of strong protic acids are not nucleophilic. Moreover, the resultant products should be ammonium salts. With this strategy, another unignorable issue is that when tertiary amines and acids coexist, they will preferentially form salts, resulting in tertiary amines losing their nucleophilicity and consequently preventing the reaction between activated alkynes and tertiary amines. (Scheme S1). Therefore, to address this problem, we proposed a strategy of tertiary amine self-initiation to facilitate the implement of click reaction of tertiary amines and activated alkynes (Scheme 1). Extra tertiary amine was added to

initiate the reaction, and the entire click reaction can then be efficiently completed through iterative cycles. According to this strategy, we first attempted the click reaction of methyl propiolate (MP), triethylamine (TEA), and trifluoroacetic acid (TFA). Ammonium salt **1** was obtained in 98% yield within 30 min by adding 10% excess TEA (Figure 1).

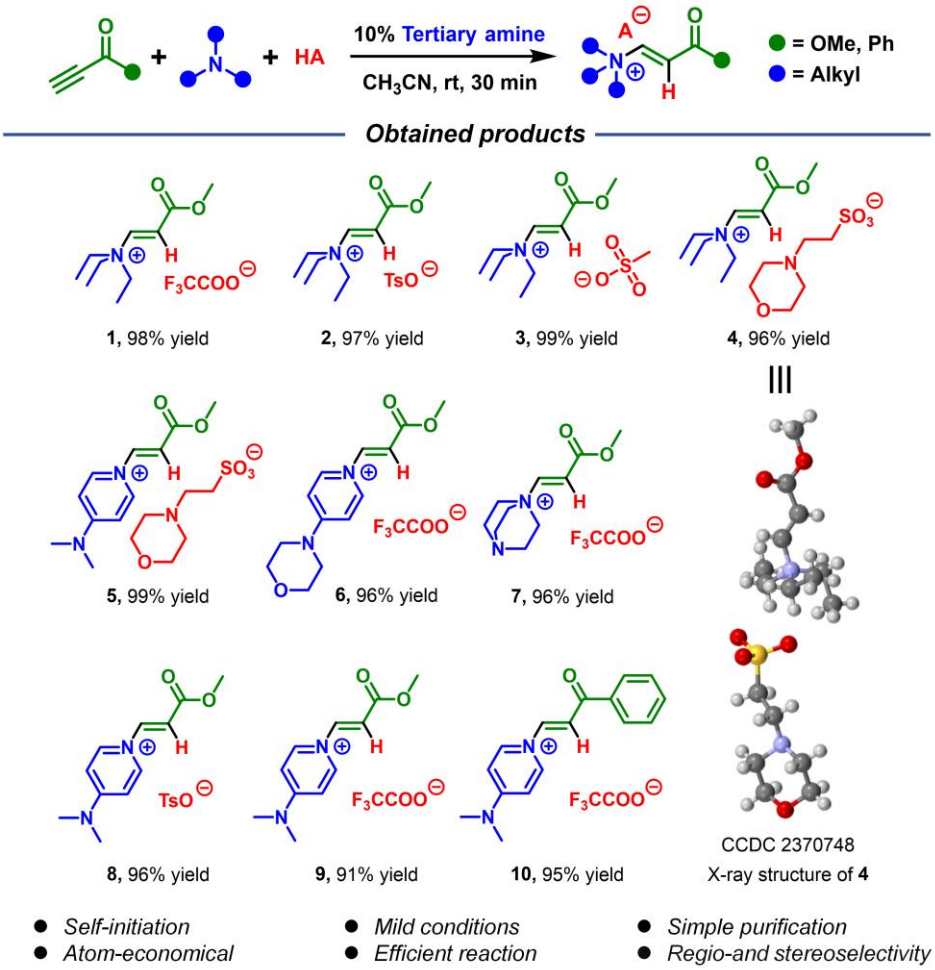

Figure 1. Click reaction of activated alkynes, tertiary amines and protic acids for the synthesis of ammonium salts and pyridinium salts.

The structures of ammonium salts were determined by ^{1}H and ^{13}C nuclear magnetic resonance (NMR) spectroscopic technique. The resonance of ethynyl protons of **1** was observed at δ 7.18 and 6.65 (J = 14.4 Hz), respectively, indicating that this reaction is an anti-Markovian *E*-addition with excellent regio- and stereoselectivity. Thanks to the high polarity of the ammonium salts, the products were quickly and conveniently purified just by sedimentation. Consequently, we also

synthesized compounds **2** to **10** in high yields (91% ~ 99%) under mild conditions (Figure 1). Moreover, the structure of ammonium salt **4** was also confirmed by single crystal analysis (Table S1). It is worth noting that using nucleophilic pyridine derivatives instead of tertiary amines can also yield pyridinium salts. This result reveals that as long as the tertiary amines or pyridine derivatives are nucleophilic, both of them can react with activated alkynes to produce corresponding ammonium or pyridinium salts, respectively.

Above results fully demonstrate the feasibility of the tertiary amine self-initiation strategy. The tertiary amine based amino-yne click reaction is highly efficient and atomically economical with excellent regio- and stereoselectivity, which provides a convenient and powerful tool for the preparation of ammonium or pyridinium salts.

Polymerization. Encouraged by the exciting results of tertiary amine based amino-yne click reaction, we attempted the click polymerizations by the same self-initiation strategy. The diyne monomers were synthesized in one-step esterification reaction (Scheme S2), and the tertiary amine monomers and protic acids are commercially available. As the monomer concentration raised, the weight average molecular weights (M_w) of the P**1a**/**2a**/**3a** gradually increased (Table S2). The M_w of the P**1a**/**2a**/**3a** ceased to increase when the concentration was 1 M. Under the conditions of tertiary amine self-initiation, the optimal monomer concentration was 1 M, and P**1a**/**2a**/**3a** with a M_w of 11,000 could be obtained in 99% yield.

It should be noted that the conditions for organic reactions are not always applicable to polymerizations. Under above tertiary amine self-initiation conditions, organic reactions can proceed very well. However, for polymerizations, excessive tertiary amine monomers can directly lead to an imbalance in the monomer equivalence ratio, which will limit the polymer chain growth and result in low M_w values (Table S3). Therefore, to further improve the polymerization result, we needed to maintain the same stoichiometric ratio of diynes and tertiary amine monomers. However, under such circumstance, the tertiary amines were completely protonated and thus not reactive. To solve this problem, we still needed to add extra bases as initiator to reproduce the tertiary amine self-initiation process. Notably, the base used here must be basic only and not

nucleophilic. Otherwise, the base initiator will react with the activated alkyne, causing end-capping and low molecular weights of the products. Therefore, after optimizing different bases, the steric hindered amine *N*,*N*-diisopropylethylamine (DIPEA) was found to have the best catalytic effect on polymerizations (Tables S3 and S4). When adding 10% DIPEA, P**1a**/**2a**/**3a** was obtained with a M_w of 18,300 in 99% yield (Table S4, entry 3). Compared with the polymerization results of tertiary amine self-initiation, DIPEA initiation indeed significantly improved the polymerization efficiency. We also used DIPEA to initiate organic reactions of TEA, TFA and MP, and the ^{1}H NMR spectrum confirmed that the product was only generated by the click reaction of TEA (Figure S1). These results indicate that DIPEA only exhibits alkalinity to initiate the reaction and does not interfere with the nucleophilic addition of tertiary amines.

For solvent optimization, we tried high polarity solvents such as dimethyl sulfoxide (DMSO), *N*,*N*-dimethylformamide (DMF) and *N*-methyl-2-pyrrolidone (NMP), and acetonitrile, the polymerization results demonstrated that the polymerization in CH_3CN displayed the best result (Table S5). Notably, the tertiary amine based amino-yne click polymerizations also showed excellent water tolerance (Table S5). Even a large amount of water was added to the reaction or pure water was directly used as the solvent, the polyelectrolytes were still obtained in high yields (up to 99%) but with decreased M_w. It suggests that water does not prevent the reaction, but only reduces the efficiency of the polymerization.

Under the optimized polymerization conditions, 15 different PAAs were synthesized with high M_w (up to 17,600) in excellent yields (up to 99%) (Table 1). When utilizing diprotic acid M**3c** for the polymerization, the resultant polymer was insoluble in water or DMF due to strong electrostatic interaction but only soluble in DMSO. The polymerization was significantly influenced by the structure of monomers. The possible reason might be that the polyelectrolyte backbones only have positive charges, which repel each other and make the polymer chain more rigid. The use of diynes with longer alkyl chains, tertiary amine monomers with ethyl substituent, and protic acids with smaller structural rigidity will result in polyelectrolyte backbones more flexible, thereby increasing the reaction possibilities of the polymer end groups and makes the polymerization more efficient.

Table 1. Polymerizations of diynes M**1** and tertiary diamines M**2** and protic acids M**3**[a].

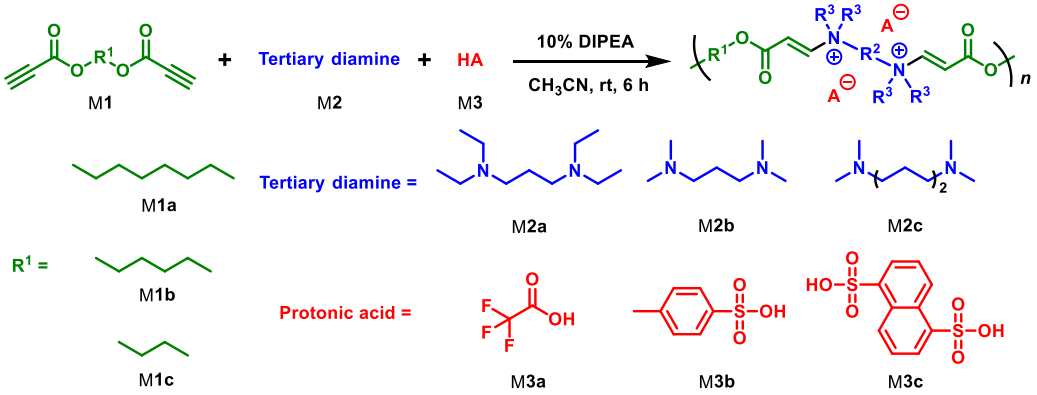

entry	polymer	yield (%)	M_n[b]	M_w[b]	$Đ$[b]
1	**P1a/2a/3a**	99	11,800	17,600	1.48
2	**P1a/2b/3a**	99	6200	7500	1.20
3	**P1a/2c/3a**	98	7600	9100	1.20
4	**P1a/2a/3b**	96	9600	13,800	1.43
5[c]	**P1a/2a/3c**	99	—	—	—
6	**P1b/2a/3a**	99	11,600	15,500	1.34
7	**P1b/2b/3a**	99	6800	9000	1.32
8	**P1b/2c/3a**	99	8200	11,000	1.33
9	**P1b/2a/3b**	99	6900	10,000	1.44
10[c]	**P1b/2a/3c**	99	—	—	—
11	**P1c/2a/3a**	98	5700	6900	1.22
12	**P1c/2b/3a**	98	5300	5800	1.09
13	**P1c/2c/3a**	99	4700	5200	1.09
14	**P1c/2a/3b**	96	5800	7200	1.25
15[c]	**P1c/2a/3c**	99	—	—	—

[a] Carried out at room temperature for 6 h in CH_3CN. [M**1**] = 1 M, [M**1**]/[M**2**]/[M**3**]/[DIPEA] = 1:1:2:0.2. [b] Determined by gel-permeation chromatography (GPC) in DMF on the basis of a linear poly(methyl methacrylate) (PMMA) calibration. Dispersity ($Đ$) = M_w/M_n. [c] Carried out at room temperature for 6 h in DMSO. [M**1**] = 0.5 M, [M**1**]/[M**2**]/[M**3**]/[DIPEA] = 1:1:1:0.2. The resultant polymers were poorly soluble in common organic solvents and the molecular weights were undetermined.

The resultant polymer structures were characterized by Fourier transform infrared (FT-IR) and NMR spectroscopies. **P1b/2a/3a** was used as an example to illustrate the correctness of the

polymer structures. In the FT-IR spectrum of P**1b**/**2a**/**3a**, the C≡C vibration peak of the diyne M**1b** at 2117 cm^{-1} completely disappeared after the polymerization, and a new C=C vibration peak of P**1b**/**2a**/**3a** appeared at 1692 cm^{-1} (Figure S3), indicating that the diyne, tertiary amine monomer, and protic acid had indeed undergo click polymerization. In the FT-IR spectra of **1** and P**1b**/**2a**/**3a**, it can be seen that their peak positions were consistent, suggesting the correctness of the polymer structure. Additionally, we also demonstrated the polymer structure more intuitively from ^{1}H and ^{13}C NMR spectrums. In the ^{1}H NMR spectrum of P**1b**/**2a**/**3a** (Figure S4A), the resonance of terminal ethynyl proton of M**1b** at δ 4.56 disappeared completely after the polymerization, and a new proton resonance with a coupling constant of 14.3 Hz appeared at δ 7.24 and δ 6.66. Comparing with **1**, the ethynyl proton peaks and coupling constant were consistent, proving the correctness of the polymer structure. In the ^{13}C NMR spectrum of P**1b**/**2a**/**3a** (Figure S4B), the C≡C resonance of M**1b** at δ 78.93 and δ 74.74 completely disappeared, and new C=C resonance peaks were observed at δ 145.57 and 122.88, which was also consistent with the ^{13}C NMR spectrum of **1**.

Above structural analysis of the resultant polyelectrolytes demonstrates that the PAAs can be successfully synthesized by the tertiary amine based amino-yne click polymerization. Detailed structural information of other polyelectrolytes can be found in supporting information.

Ionic Clusteroluminescence. Charged groups endow the polyelectrolytes with many unique properties that are different from conventional polymers. Depending on through-space interaction (TSI),[43-45] many small molecules and polymers without conjugated structures can emit efficiently.[46-48] Compared to conventional polymers, there are large number of anions and cations in PAAs, so there will be stronger electrostatic interactions among polymer chains, which means that PAAs can also exhibit nontraditional luminescence.

Aiming to uncover the unique nontraditional luminescence of PAAs, we explored the photophysical properties of compounds **1** and **2**. The results show that the anions in AAs had little influence on the absorption and emission peaks (Figures S5 and S6), but they can significantly affect quantum yields (QY) (Figure S7). Similarly, the QY of P**1b**/**2a**/**3b** was much lower than that

of P**1b**/**2a**/**3a** when the anion was changed (Figure S7). These results suggest that the anions indeed participate in and impact the luminescence of the AAs. Since the oxygen anion is electron-rich, it is reasonable to speculate that the AAs are emissive with its anion as the electron donor. For electron acceptor, the electrically deficient acrylate groups of the cation most likely play this role. Compound **11** was used to prove this conjecture. In the absorption spectrum of **11**, there is no obvious absorption even at the high concentration of 1×10^{-2} M (Figure S8). When the cationic part contains no acrylate group, there is no emission. This result is in sharp contrast to the absorption and emission of **1** (Figure S5), which fully demonstrates that the electrically deficient acrylate group is an essential part for the luminescence of AAs, proving that it acts as electron acceptor for the emission. According to the above analysis, we have clarified that the VASs implement its emission through the acrylate group of cation and the oxygen negative ion of anion as the electron acceptor and electron donor, respectively. The luminescence of AAs can only be achieved through TSI, as there are no traditional conjugated structures. Interestingly, small molecules and polymers both feature superior luminescence efficiency, suggesting that the electrostatic interaction of cations and anions greatly increases the possibility of TSI between the acrylate group and oxygen negative ion. This interaction enables the intrinsic structure of AAs to emit efficiently.

Subsequently, we found that the emission phenomena of small molecules and polymers are significantly different, which implies that they have distinct luminescence mechanism (Figure 2). At different concentrations, the main absorption wavelengths (λ_{abs}) of **1** are all shorter than 300 nm, which belongs to the intrinsic absorbance of AAs. However, when the concentration is higher than 5×10^{-3} M, there appeared a new λ_{abs} at 340 nm (Figure 2A). For the excitation spectrum of **1**, regardless of concentration increases, the optimal excitation wavelength (λ_{ex}) is located at 370 nm (Figure 2B), which corresponds to the optimal excitation wavelength for the intrinsic structure of VAS. But when the concentration is greater than 5×10^{-3} M, a weak shoulder peak appeared at 397 nm, which is corresponding with the λ_{abs} at 340 nm. This result indicates that small molecules only show luminescence at high concentrations, but the main luminescence always originates from

the intrinsic structure of AAs. In the photoluminescence (PL) spectra of **1** at different λ_{ex}, there was no obvious excitation-dependent emission (EDE) effect at high concentration (Figure 2C), which demonstrates that AAs are very difficult to aggregate and luminescent with its own intrinsic structure. **2** also displays similar photophysical properties (Figure S6).

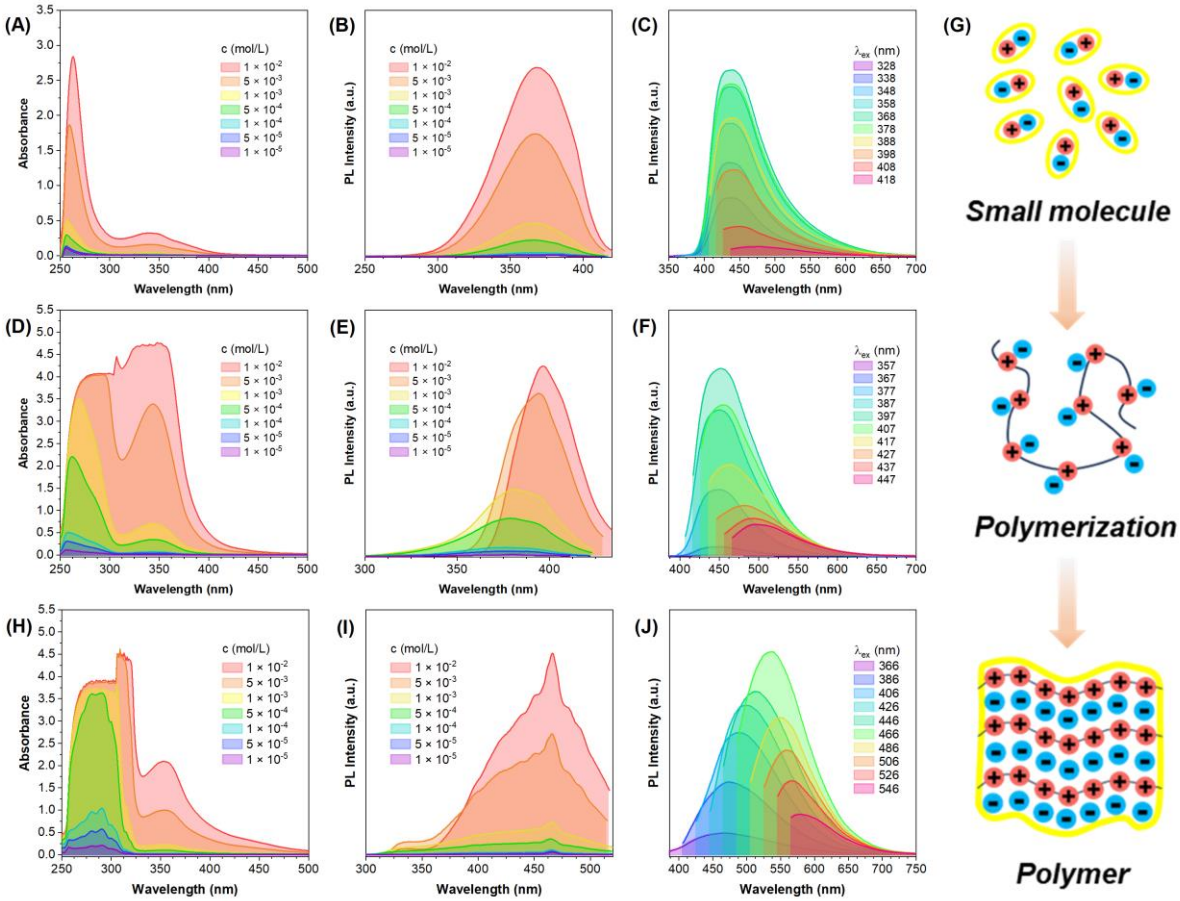

Figure 2. (A) Concentration-dependent UV-vis absorption spectrums, (B) excitation spectrums and (C) excitation-dependent photoluminescence (PL) spectrums (c = 1 × 10^{-2} M) of model compound **1** in DMSO. (D) Concentration-dependent UV-vis absorption spectrums, (E) excitation spectrums and (F) excitation-dependent PL spectrums (c = 1 × 10^{-2} M) of P**1a**/**2c**/**3a** in DMSO. (G) Schematic representation of different luminescence mechanisms between small molecule and polymer. (H) Concentration-dependent UV-vis absorption spectrums, (I) excitation spectrums and (J) excitation-dependent PL spectrums (c = 1 × 10^{-2} M) of P**1b**/**2a**/**3c** in DMSO.

Interestingly, even at low concentration, P**1a**/**2c**/**3a** exhibited a λ_{abs} at 340 nm (Figure 2D). With the concentration gradually increasing, the λ_{ex} of P**1a**/**2c**/**3a** shifted from 370 to 397 nm (Figure

2E). In the PL spectrums of P**1a**/**2c**/**3a** at different λ_{ex}, P**1a**/**2c**/**3a** exhibited more evident EDE effect compared to small molecules (Figure 2F). As the λ_{ex} redshifted, the emission wavelength (λ_{em}) of P**1a**/**2c**/**3a** also redshifted, which is consistent with clusteroluminescence (CL).[49-52] The fundamentally different luminescence mechanisms of small molecules and polymers are due to their different degrees of aggregation. AAs can dissolve well in high polarity solvents. Under the overall electrostatic field, it will be uniformly dispersed in the solution. Although there is little aggregation at high concentrations of small molecules, their aggregate are very easily broken by solvent molecules. Therefore, AAs are mainly luminescent with their intrinsic structures. While for polymers, the polymer chains link the AA units through covalent bonds. Through the polymerization, the positive charges are like beads strung together and significantly brought closer to each other, which breaks the electrostatic equilibrium of the cations and results in a higher density of positive charges along the polymer chains. This imbalance in charge density enhances the electrostatic interaction between polyelectrolytes, making them easier to form stable ionic clusters than the small molecules, and thus generates luminescence (Figure 2G). We have tested photophysical properties of other PAAs (Figures S9-S16), and the results are consistent with the above analysis.

According to above analysis, we hypothesized that changing anions can regulate the photophysical properties of PAAs. Consequently, we carried out photophysical measurement on P**1b**/**2a**/**3b**. Compared with P**1b**/**2a**/**3a** (Figure S10A), when *p*-toluene sulfonic acid anion (TsO^-) was introduced, the λ_{em} of P**1b**/**2a**/**3b** red-shifted and a more significant EDE effect was observed (Figure S17A), but its QY dramatically decreased (Figure S7). This result illustrates that steric hindrance of larger anions can also restrain polymer aggregation and make it more difficult to form ionic clusters, subsequently diminishing the luminescence efficiency of PAA.s This conclusion was also confirmed by the weaker absorption intensity of P**1b**/**2a**/**3b** at 340 nm than that of P**1b**/**2a**/**3a** (Figures S10C and S17C). Moreover, bifunctional naphthalene disulfonic acid was used to prepare P**1b**/**2a**/**3c**. Theoretically, the bifunctional anions would pull the polymer chains together, making the ionic clusters easier to form, making λ_{ex} and λ_{em} more red-shifted. The fluorescence of

P**1b**/**2a**/**3c** indeed exhibited a significant redshift compared with P**1b**/**2a**/**3a**, and the λ_{ex} was shifted from 394 to 466 nm and the λ_{em} from 450 to 534 nm, presenting a stronger EDE effect (Figures 2H-J and S18). Meanwhile, the QY value of P**1b**/**2a**/**3c** was recorded to be 14.4% in thin film state (Figure S7), confirming that the strategy of introducing bifunctional anions is very successful. Notably, P**1a**/**2a**/**3c** and P**1c**/**2a**/**3c** also displayed comparable photophysical properties (Figures S19 and S20).

Furthermore, different luminescence behaviors of small molecules and polymers were experimentally demonstrated. **12** appeared a redshift in λ_{ex} and λ_{em} compared to **1** (Figure S21), suggesting that the dispersed small molecules are attracted by bifunctional anions, increasing the possibility of aggregation and ultimately altering their luminescence. Additionally, small molecules and polymers have similar λ_{ex} and λ_{em} at the concentration of 1×10^{-5} M (Figures S22-S24), suggesting that they have same emissive unit. At extremely dilute concentration, the polymer cannot aggregate, hence they will return to the intrinsic luminescence of the AAs. Moreover, with the alkyl chain length of diynes becoming short, the corresponding QY of the PAAs decreased (Figure S7) because longer alkyl chains enable the polymers more flexible and facilitating the formation of ionic clusters, and in turn enhancing the emission.

Degradation and Reconstruction of PAA. Theoretically, the tertiary amine of AAs is easily substituted by other nucleophilic reagents owing to its attachment to electrically deficient *β*-acrylate group. We therefore explored the precise degradation and backbone reconstruction of PAAs (Figure 3A). Because the thiol groups will generate sulfur anions with strong nucleophilicity under basic conditions, we first attempted the precise degradation of P**1b**/**2a**/**3b** by 4-methylbenzenethiol under basic conditions. The ^{1}H NMR spectrum of the degradation solution (Figure S25) showed that the characteristic C=C proton resonance of P**1b**/**2a**/**3b** at δ 7.21 and 6.65 thoroughly disappeared, while those belonging to the addition product D**1** of 4-methylbenzenethiol and M**1b** appeared at δ 7.82 and 5.46, respectively,[53] suggesting that the P**1b**/**2a**/**3b** had been completely degraded. Notably, the degradation only took 30 min in CH_3CN at room temperature, illustrating the high efficiency of the nucleophilic substitution of tertiary amines by thiophenols.

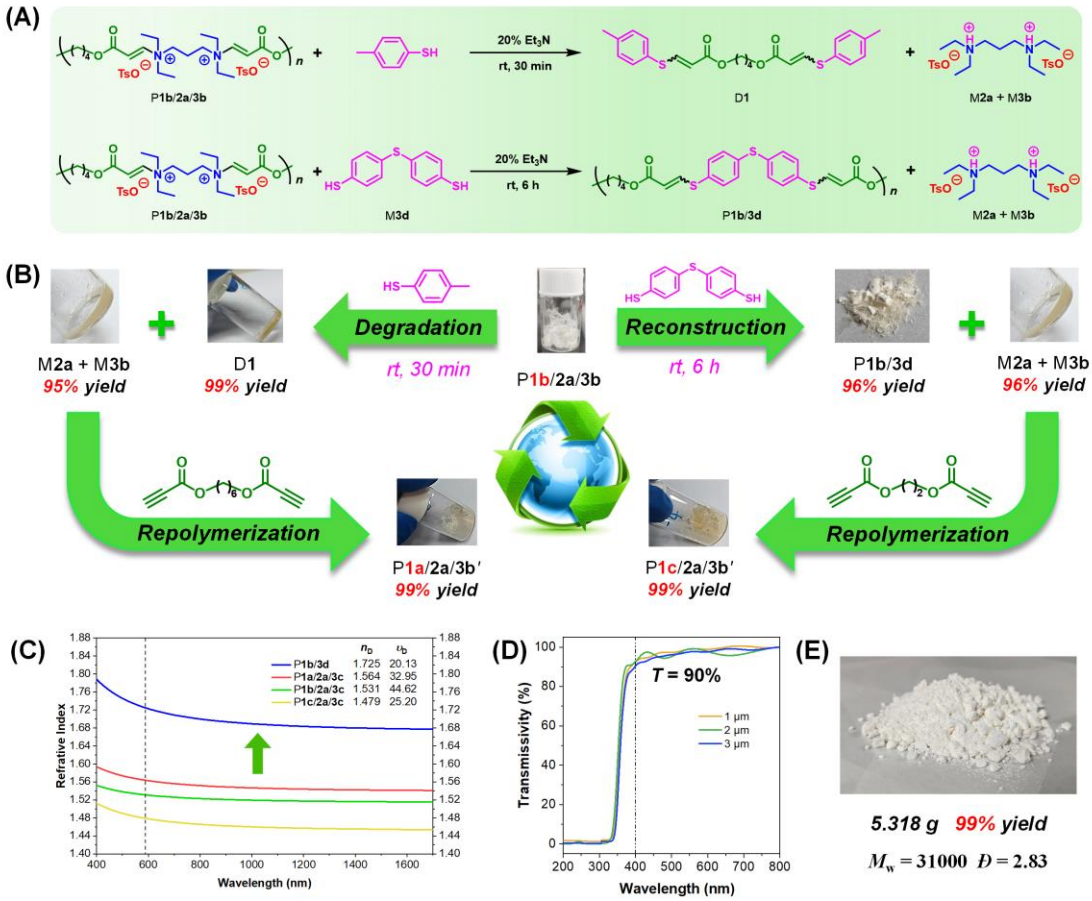

Figure 3. (A) Reactions of PAA degradation and reconstruction. Degradation was carried out at room temperature for 30 min in CH_3CN. [PAA]/[*p*-toluenethiol]/[Et_3N] = 1:2:0.2. [PAA] = 0.1 M. Reconstruction was carried out at room temperature for 6 h in the mixture of CH_3CN and $CHCl_3$ (v/v = 1/3). [PAA]/[M**3d**]/[Et_3N] = 1:1:0.2. [PAA] = 0.1 M. (B) Schematic illustration of the recycling of PAA through polymer degradation and reconstruction. (C) The refractive index of P**1b**/**3d** and PAA vs wavelength. (D) UV-vis transmission spectra of P**1b**/**3d** films with varying thicknesses (1, 2 and 3 μm) on glass substrate. (E) Gram-scale reconstruction of PAA toward P**1b**/**3d′**.

Thanks to the significant difference in polarity of degradation products, we separated and purified the degradation products just by sedimentation in low polarity solvent. The product D**1** and the mixture of M**2a** and M**3b** were obtained in 99% and 95% yields, respectively. Their structures were fully characterized by ^{1}H NMR spectra (Figures S26 and S27). Prominently, the proton resonance of the two products are exactly identical with the degradation solution (Figure

S28). The separated mixture of M**2a** and M**3b** can also be used as raw materials to re-polymerize with M**1a**, and finally yielded P**1a**/**2a**/**3b′** with M_w of 11,600 in 99% yield (Figure S29). These results are similar to those of P**1a**/**2a**/**3b** (Table 1, entry 4).

Next, we utilized dithiophenol M**3d** to reconstruct the polymer backbone (Figure 3B). After reacting for 6 h at room temperature, we successfully realized the replacement of P**1b**/**2a**/**3b** backbone under basic conditions and obtained P**1b**/**3d** with M_w of 25,000 in 96% yield (Figure S30). P**1b**/**3d** showed excellent optical properties with higher refractive index (Δn = 0.2) than P**1b**/**2a**/**3c**. Its refractive index at 589.3 nm can be as high as 1.73 and the Abbé number is 20.13 (Figure 3C). Notably, even the film thickness reaches 3 μm, the transmittance at visible light region can still higher than 90% (Figure 3D). These results demonstrate that P**1b**/**3d** is a high-performance refractive material that benefits from the introduction of thiophenol M**3d**.[28,53,54]

In addition, we also conducted gram-scale synthesis of polymers by this efficient substitution process. Ultimately, 5.32 g of P**1b**/**3d′** was prepared with a high yield (up to 99%) (Figure 3E). Meanwhile, its refractive index, Abbé number, and transparency are similar to P**1b**/**3d** (Figures S31 and S32). The mixture of M**2a** and M**3b** obtained in 96% yield from the reconstruction process (Figure S33) could be re-polymerized with M**1c**, from which P**1c**/**2a**/**3b′** was furnished in 99% yield (Figure S34). Remarkably, under the same basic conditions (20% Et_3N), P**1b**/**3d** prepared by backbone reconstruction possess significantly better solubility than those synthesized by the polymerization of M**1b** and M**3d** (Figure S35). This means that the substitution process is more controllable for the polymerization.

Utilizing the *in situ* substitution strategy, we can efficiently achieve precise degradation of PAAs or introduce different functional units into the polymer backbone. Moreover, after degradation or reconstruction, tertiary amine monomers and protic acids can be recycled, which can repolymerize with different diynes to prepare another PAAs with diverse structures. These results fully demonstrate the excellent degradation and reconstruction properties of PAAs, which is very much in line with the concept of green chemistry.

Adhesive Ability of PAAs. Abundant electrostatic interaction and adjustable thermodynamic

properties of PAAs makes them promising for adhesive applications (Figures S36 and S37). We first tested the adhesive property of P**1b**/**2a**/**3c** on glass, plastic, and stainless steel after 6 h at 80 ℃(Figure 4A).Unfortunately, P**1b**/**2a**/**3c** did not show desired adhesive strength (Figure 4B).[55] Therefore, amino acid rich in hydrogen bonds was introduced into anions to further enhance the interaction between polymers and substrates. More importantly, amino acids could form hydrogen bonds and generate amino cations and carboxyl anions, which are very compatible with PAAs. We synthesized P**1a**/**2a**/**3e**, P**1d**/**2a**/**3e**, and P**1e**/**2a**/**3e** by using *L*-cysteic acid M**3e** as protic acid and tested their adhesive property. The lap shear adhesion tests showed that P**1d**/**2a**/**3e** had a significantly better adhesive ability, and its maximum adhesive strength to brass can reach 5.6 MPa, which was 7 times higher than the other two polyelectrolytes (Figure S38).

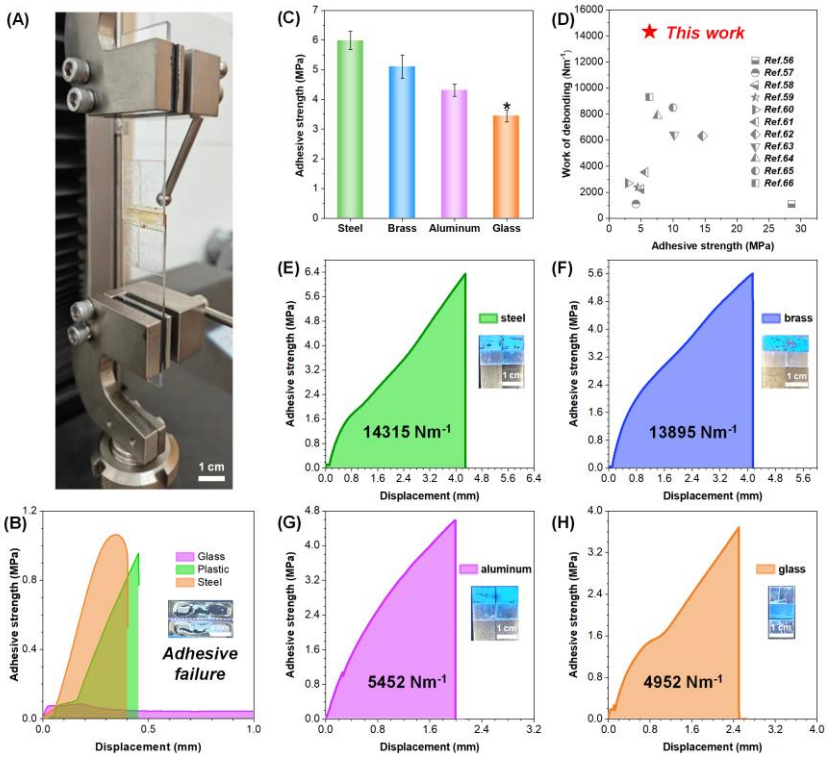

Figure 4. (A) Photogragh of the lap shear test. (B) Adhesive strength vs displacement for P**1b**/**2a**/**3c** on glass, plastic and steel substrates. Adhesive area is 120 mm^2 (24 mm ×5 mm). (C) Adhesive strengths of P**1d**/**2a**/**3e** on steel, brass, aluminum and glass substrates. All error bars represent the standard deviation with at least three replicates. (D) Comparison of P**1d**/**2a**/**3e** with previously reported strong and tough adhesives in the work of de-bonding and lap shear strength

on steel substrate. (E)-(H) Adhesive strength vs displacement for P**1d**/**2a**/**3e** on steel, brass, aluminum and glass substrates. Inset: the photo of adhesive surface after failure under 365 nm light irradiation. Adhesive area is 60 mm^2 (10 mm ×6 mm).

Since PAAs are highly efficient in clusteroluminescence, we can judge the failure mode of the adhesives with the help of emission (Figure S39). The failed strips of P**1a**/**2a**/**3e** exhibited a massive peeling, suggesting that there was a weak interaction between P**1a**/**2a**/**3e** and the substrate. The reason may be that the shorter carbon chains result in a stiffer polymer, thereby diminishing the likelihood of the polymer chains interacting with the substrate surface. The strips adhered by P**1e**/**2a**/**3e** was uniformly distributed on the two failed surfaces (Figure S39). This result indicates that P**1e**/**2a**/**3e** possesses a good affinity for the substrate, but the insufficient cohesion of P**1e**/**2a**/**3e** leads to failure within the adhesive layer, suggesting that the long alkyl chains are also not conducive to the adhesive strength. The reason might be that the alkyl chains with low polarity can easily cleave the ionic and hydrogen bonds within the polymer, thereby reducing the cohesion and strength of the adhesive.

The adhesive strength of P**1d**/**2a**/**3e** on stainless steel, brass, aluminum, and glass could reach 6.4, 5.6, 4.6 a, and 3.6 MPa, respectively (Figure 4C). When utilized glass substrate, the strip sustained damage, whereas the bonding place remained intact. Interestingly, P**1d**/**2a**/**3e** adhesive performed significant displacement before failure and its work of de-bonding for stainless steel can reach an astonishing 14315 Nm^{-1}. It is worth noting that the work of debonding of P**1d**/**2a**/**3e** is far ahead of many other adhesives (Figure 4D and Table S6),[56-66] which means this polymer possesses excellent adhesive properties. Moreover, this polymer also exhibited significant work of debonding for other substrates (Figure 4E-H), demonstrating that the strategy of introducing amino acids into PAAs is very effective for strengthening the adhesive property.

The reason for this excellent adhesive property of P**1d**/**2a**/**3e** was explored. The degradation and reconstruction results of PAAs suggests that the polymer is reactive and prone to nucleophilic substitution when encountering nucleophilic reagents. Consequently, P**1d**/**2a**/**3e** might also partially react with the hydroxyl groups on the substrate surface during bonding, thereby forming

a certain degree of covalent bond with the substrates. To verify the hypothesis, we washed the surface of stainless steel after adhesive failure using methanol and deionized water. Under 365 nm UV light irradiation, no blue fluorescence was observed, indicating that we had successfully cleaned the polymer physically adhering on the substrate. While, according to the FT-IR spectra, the adhered surface appeared vibration signals belonging to β-ammonium acrylate moiety (Figure S40). This result showed that P**1d**/**2a**/**3e** could not only physically adhere on the substrate, but also chemically bond with the surface through the substitution reaction of hydroxyl groups and PAAs.

CONCLUSIONS

In this work, a tertiary amine-based amino-yne click polymerization was established via the tertiary amine self-initiation strategy. The polymerization of activated alkynes, tertiary amine monomers and protic acid efficiently furnishes PAAs with diverse structures. The resultant PAAs exhibit ionic cluster luminescence, and the emission could be fine-tuning by anions. Moreover, thanks to the reactive β-tertiary amino acrylate moiety in PAAs, they could further react with thiol groups to make them degraded or reconstructed. Notably, the reconstructed PAAs could show refractive indices enhancement of 0.2. Thanks to the reactive PAAs and their containing amino acid units, the polymers show interesting adhesive property, and the adhesive strength and work of debonding of the PAA on stainless steel could reach 6.4 MPa and 14315 Nm^{-1}, respectively. Thus, this work not only established a new amino-yne click polymerization, but also provided novel kind of polyelectrolytes with multiple properties.

AUTHOR INFORMATION

Corresponding Author

*Anjun Qin − State Key Laboratory of Luminescent Materials and Devices, Guangdong Provincial Key Laboratory of Luminescence from Molecular Aggregates, Center for Aggregation-Induced Emission, AIE Institute, South China University of Technology, Guangzhou 510640, China; E-mail: msqinaj@scut.edu.cn

ORCID

AnjunQin: https://orcid.org/0000-0001-7158-1808.

Notes

The authors declare no competing financial interest.

ACKNOWLEDGMENT

This work was financially supported by the National Natural Science Foundation of China (21788102), the Natural Science Foundation of Guangdong Province (2023B1212060003), and the Innovation and Technology Commission of Hong Kong (ITC-CNERC14SC01).

REFERENCES

(1). Li, F.; Mao, X.; Li, F.; Li, M.; Shen, J.; Ge, Z.; Fan, C.; Zuo, X. Ultrafast DNA Sensors with DNA Framework-Bridged Hybridization Reactions. *J Am Chem Soc*. **2020**, *142*, 9975-9981.

(2). Li, Z.; Wang, C.; Li, J.; Zhang, J.; Fan, C.; Willner, I.; Tian, H. Functional DNA Structures and Their Biomedical Applications. *CCS Chem*. **2020**, *2*, 707-728.

(3). Xu, W.; Hu, F.; Li, J.; Shang, J.; Liu, X.; Zeng, Y.; Wu, Q.; Wang, F. External Stimulation-Controlled Dynamic DNA Devices for Biosensing and Biomedical Applications. *Sci China Chem*. **2023**, *66*, 3105-3115.

(4). Liu, C.; Luo, J. Protein Oligomer Engineering: A New Frontier for Studying Protein Structure, Function, and Toxicity. *Angew. Chem. Int. Ed*. **2023**, *62*, e202216480.

(5). Xu, Q.; Ma, Y.; Sun, Y.; Li, D.; Zhang, X.; Liu, C. Protein Amyloid Aggregate: Structure and Function. *Aggregate*. **2023**, *4*, e333.

(6). Quek, G.; Roehrich, B.; Su, Y.; Sepunaru, L.; Bazan, G. C. Conjugated Polyelectrolytes: Underexplored Materials for Pseudocapacitive Energy Storage. *Adv. Mater*. **2021**, *34*, 2104206.

(7). Tong, Y.; Xu, B.; Ye, F. Recent Advance in Solution-Processed Hole Transporting Materials

for Organic Solar Cells. *Adv. Funct. Mater*. **2023**, *34*, 2310865.

(8). Yang, L.; Shen, S.; Chen, X.; Wei, H.; Xia, D.; Zhao, C.; Zhang, N.; Hu, Y.; Li, W.; Xin, H.; Song, J. Doped/Undoped A1-A2 Typed Copolymers as ETLs for Highly Efficient Organic Solar Cells. *Adv. Funct. Mater*. **2023**, *33*, 2303603.

(9). Keene, S. T.; Laulainen, J. E. M.; Pandya, R.; Moser, M.; Schnedermann, C.; Midgley, P. A.; McCulloch, I.; Rao, A.; Malliaras, G. G. Hole-Limited Electrochemical Doping in Conjugated Polymers. *Nat. Mater*. **2023**, *22*, 1121-1127.

(10). Wang, H.; Yang, Y.; Zhang, Y.; Wang, S.; Tan, Z. a.; Yan, S.; Wang, L.; Hou, J.; Xu, B. p—π Conjugated Polyelectrolytes Toward Universal Electrode Interlayer Materials for Diverse Optoelectronic Devices. *Adv. Funct. Mater*. **2023**, *33*, 2213914.

(11). Zhang, C.; Liu, X.; Gong, J.; Zhao, Q. Liquid Sculpture and Curing of Bio-Inspired Polyelectrolyte Aqueous Two-Phase Systems. *Nat. Commun*. **2023**, *14*, 2456.

(12). Li, C.; Cheng, J.; He, Y.; He, X.; Xu, Z.; Ge, Q.; Yang, C. Polyelectrolyte Elastomer-Based Ionotronic Sensors with Multi-Mode Sensing Capabilities via Multi-Material 3D Printing. *Nat. Commun*. **2023**, *14*, 4853.

(13). Li, T.; Li, X.; Yang, J.; Sun, H.; Sun, J. Healable Ionic Conductors with Extremely Low-Hysteresis and High Mechanical Strength Enabled by Hydrophobic Domain-Locked Reversible Interactions. *Adv. Mater*. **2023**, *35*, 2307990.

(14). Pace, G. T.; Le, M. L.; Clément, R. J.; Segalman, R. A. A Coacervate-Based Mixed-Conducting Binder for High-Power, High-Energy Batteries. *ACS Energy Lett*. **2023**, *8*, 2781-2788.

(15). He, Y.; Cheng, Y.; Yang, C.; Guo, C. F. Creep-Free Polyelectrolyte Elastomer for Drift-Free Iontronic Sensing. *Nat. Mater*. **2024**.

(16). He, W.; Wang, M.; Mei, G.; Liu, S.; Khan, A. Q.; Li, C.; Feng, D.; Su, Z.; Bao, L.; Wang, G.; Liu, E.; Zhu, Y.; Bai, J.; Zhu, M.; Zhou, X.; Liu, Z. Establishing Superfine Nanofibrils for Robust Polyelectrolyte Artificial Spider Silk and Powerful Artificial Muscles. *Nat. Commun*. **2024**, *15*, 3485.

(17). Nguyen, V. H.; Oh, S.; Mahato, M.; Tabassian, R.; Yoo, H.; Lee, S.-G.; Garai, M.; Kim, K.

J.; Oh, I.-K. Functionally Antagonistic Polyelectrolyte for Electro-Ionic Soft Actuator. *Nat. Commun*. **2024**, *15*, 435.

(18). So, R. C.; Carreon-Asok, A. C. Molecular Design, Synthetic Strategies, and Applications of Cationic Polythiophenes. *Chem. Rev*. **2019**, *119*, 11442-11509.

(19). Zeng, Y.; Zhou, X.; Qi, R.; Dai, N.; Fu, X.; Zhao, H.; Peng, K.; Yuan, H.; Huang, Y.; Lv, F.; Liu, L.; Wang, S. Photoactive Conjugated Polymer-Based Hybrid Biosystems for Enhancing Cyanobacterial Photosynthesis and Regulating Redox State of Protein. *Adv. Funct. Mater*. **2020**, *31*, 2007814.

(20). Aili, D.; Yang, J.; Jankova, K.; Henkensmeier, D.; Li, Q. From Polybenzimidazoles to Polybenzimidazoliums and Polybenzimidazolides. *J. Mater. Chem. A*. **2020**, *8*, 12854-12886.

(21). Qi, R.; Zhao, H.; Zhou, X.; Liu, J.; Dai, N.; Zeng, Y.; Zhang, E.; Lv, F.; Huang, Y.; Liu, L.; Wang, Y.; Wang, S. In Situ Synthesis of Photoactive Polymers on a Living Cell Surface via Bio-Palladium Catalysis for Modulating Biological Functions. *Angew. Chem. Int. Ed*. **2021**, *60*, 5759-5765.

(22). Tian, S.; Yue, Q.; Liu, C.; Li, M.; Yin, M.; Gao, Y.; Meng, F.; Tang, B. Z.; Luo, L. Complete Degradation of a Conjugated Polymer into Green Upcycling Products by Sunlight in Air. *J Am Chem Soc*. **2021**, *143*, 10054-10058.

(23). Anderson, C. L.; Dai, N.; Teat, S. J.; He, B.; Wang, S.; Liu, Y. Electronic Tuning of Mixed Quinoidal-Aromatic Conjugated Polyelectrolytes: Direct Ionic Substitution on Polymer Main-Chains. *Angew. Chem. Int. Ed*. **2019**, *58*, 17978-17985.

(24). Wang, K.; Liu, J.; Liu, P.; Wang, D.; Han, T.; Tang, B. Z. Multifunctional Fluorescent Main-Chain Charged Polyelectrolytes Synthesized by Cascade C-H Activation/Annulation Polymerizations. *J Am Chem Soc*. **2023**, *145*, 4208-4220.

(25). He, B.; Li, Y.; Li, M.; Kang, M.; Liu, X.; Huang, J.; Wang, D.; Lam, J. W. Y.; Tang, B. Z. Pyridinium-Yne Click Polymerization: A Facile Strategy toward Functional Poly(Vinylpyridinium Salt)s with Multidrug-Resistant Bacteria Killing Ability. *Angew. Chem. Int. Ed*. **2024**, e202405030.

(26). Kolb, H. C.; Finn, M. G.; Sharpless, K. B. Click Chemistry: Diverse Chemical Function from

A Few Good Reactions. *Angew. Chem. Int. Ed*. **2001**, *40*, 2004-2021.

(27). Fu, X.; Qin, A.; Tang, B. Z. X-Yne Click Polymerization. *Aggregate*. **2023**, *4*, e350.

(28). Zhang, J.; Bai, T.; Liu, W.; Li, M.; Zang, Q.; Ye, C.; Sun, J. Z.; Shi, Y.; Ling, J.; Qin, A.; Tang, B. Z. All-Organic Polymeric Materials with High Refractive Index and Excellent Transparency. *Nat. Commun*. **2023**, *14*, 3524.

(29). Song, B.; Bai, T.; Liu, D.; Hu, R.; Lu, D.; Qin, A.; Ling, J.; Tang, B. Z. Visualized Degradation of CO_2-Based Unsaturated Polyesters toward Structure-Controlled and High-Value-Added Fluorophores. *CCS Chem*. **2022**, *4*, 237-249.

(30). Song, B.; Zhang, R.; Hu, R.; Chen, X.; Liu, D.; Guo, J.; Xu, X.; Qin, A.; Tang, B. Z. Site-Selective, Multistep Functionalizations of CO_2-Based Hyperbranched Poly(alkynoate)s toward Functional Polymetric Materials. *Adv. Sci*. **2020**, *7*, 2000465.

(31). Zhang, Y.; Shen, J.; Hu, R.; Shi, X.; Hu, X.; He, B.; Qin, A.; Tang, B. Z. Fast Surface Immobilization of Native Proteins through Catalyst-Free Amino-Yne Click Bioconjugation. *Chem. Sci*. **2020**, *11*, 3931-3935.

(32). He, B.; Zhang, J.; Wang, J.; Wu, Y.; Qin, A.; Tang, B. Z. Preparation of Multifunctional Hyperbranched Poly(*β*-aminoacrylate)s by Spontaneous Amino-yne Click Polymerization. *Macromolecules*. **2020**, *53*, 5248-5254.

(33). Wang, K.; Si, H.; Wan, Q.; Wang, Z.; Qin, A.; Tang, B. Z. Luminescent Two-Way Reversible Shape Memory Polymers Prepared by Hydroxyl-Yne Click Polymerization. *J. Mater. Chem. C*. **2020**, *8*, 16121-16128.

(34). He, B.; Su, H.; Bai, T.; Wu, Y.; Li, S.; Gao, M.; Hu, R.; Zhao, Z.; Qin, A.; Ling, J.; Tang, B. Z. Spontaneous Amino-yne Click Polymerization: A Powerful Tool toward Regio- and Stereospecific Poly(*β*-aminoacrylate)s. *J Am Chem Soc*. **2017**, *139*, 5437-5443.

(35). Chen, X.; Bai, T.; Hu, R.; Song, B.; Lu, L.; Ling, J.; Qin, A.; Tang, B. Z. Aroylacetylene-Based Amino-Yne Click Polymerization toward Nitrogen-Containing Polymers. *Macromolecules*. **2020**, *53*, 2516-2525.

(36). Chen, X.; Hu, R.; Qi, C.; Fu, X.; Wang, J.; He, B.; Huang, D.; Qin, A.; Tang, B. Z.

Ethynylsulfone-Based Spontaneous Amino-yne Click Polymerization: A Facile Tool toward Regio- and Stereoregular Dynamic Polymers. *Macromolecules*. **2019**, *52*, 4526-4533.

(37). Chen, J.; Xu, X.; Xia, Q.; Wang, J.; Qin, A.; Tang, B. Z. Solvent and Water Enabled Control of Alkyne-Base Polymerization Triggered by a Spontaneous Imine-Yne Click Reaction. *Macromolecules*. **2024**, *57*, 1970-1978.

(38). Han, T.; Chen, S.; Wang, X.; Fu, X.; Wen, H.; Wang, Z.; Wang, D.; Qin, A.; Yang, J.; Tang, B. Z. Autonomous Visualization of Damage in Polymers by Metal-Free Polymerizations of Microencapsulated Activated Alkynes. *Adv. Sci*. **2022**, *9*, 2105395.

(39). Bell, C. A.; Yu, J.; Barker, I. A.; Truong, V. X.; Cao, Z.; Dobrinyin, A. V.; Becker, M. L.; Dove, A. P. Independent Control of Elastomer Properties through Stereocontrolled Synthesis. *Angew. Chem. Int. Ed*. **2016**, *55*, 13076-13080.

(40). Worch, J. C.; Weems, A. C.; Yu, J.; Arno, M. C.; Wilks, T. R.; Huckstepp, R. T. R.; O'Reilly, R. K.; Becker, M. L.; Dove, A. P. Elastomeric Polyamide Biomaterials with Stereochemically Tuneable Mechanical Properties and Shape Memory. *Nat. Commun*. **2020**, *11*, 3250.

(41). Shi, Y.; Bai, T.; Qin, A.; Bai, W.; Wang, Z.; Chen, M.; Ling, J.; Tang, B. Z. Phenol-yne Click Polymerization: An Efficient Technique to Facilely Access Regio-and Stereoregular Poly(vinylene ether ketone)s. *Chem. Eur.J*. **2017**, *23*, 10725-10731.

(42). Si, H.; Wang, K.; Song, B.; Qin, A.; Tang, B. Z. Organobase-Catalysed Hydroxyl-Yne Click Polymerization. *Polym. Chem*. **2020**, *11*, 2568-2575.

(43). Zhang, H.; Tang, B. Z. Through-Space Interactions in Clusteroluminescence. *JACS Au*. **2021**, *1*, 1805-1814.

(44). Chu, B.; Zhang, H.; Hu, L.; Liu, B.; Zhang, C.; Zhang, X.; Tang, B. Z. Altering Chain Flexibility of Aliphatic Polyesters for Yellow-Green Clusteroluminescence in 38 % Quantum Yield. *Angew. Chem. Int. Ed*. **2021**, *61*, e202114117.

(45). Zhang, J.; Hu, L.; Zhang, K.; Liu, J.; Li, X.; Wang, H.; Wang, Z.; Sung, H. H. Y.; Williams, I. D.; Zeng, Z.; Lam, J. W. Y.; Zhang, H.; Tang, B. Z. How to Manipulate Through-Space Conjugation and Clusteroluminescence of Simple AIEgens with Isolated Phenyl Rings. *J. Am.*

Chem. Soc. **2021**, *143*, 9565-9574.

(46). Tang, S.; Yang, T.; Zhao, Z.; Zhu, T.; Zhang, Q.; Hou, W.; Yuan, W. Z. Nonconventional Luminophores: Characteristics, Advancements and Perspectives. *Chem. Soc. Rev*. **2021**, *50*, 12616-12655.

(47). Liu, B.; Zhang, H.; Liu, S.; Sun, J.; Zhang, X.; Tang, B. Z. Polymerization-Induced Emission. *Mater. Horiz*. **2020**, *7*, 987-998.

(48). Liao, P.; Huang, J.; Yan, Y.; Tang, B. Z. Clusterization-Triggered Emission (CTE): One for All, All for One. *Mater. Chem. Front*. **2021**, *5*, 6693-6717.

(49). Chu, B.; Liu, X.; Xiong, Z.; Zhang, Z.; Liu, B.; Zhang, C.; Sun, J. Z.; Yang, Q.; Zhang, H.; Tang, B. Z.; Zhang, X.-H. Enabling Nonconjugated Polyesters Emit Full-Spectrum Fluorescence from Blue to Near-Infrared. *Nat. Commun*. **2024**, *15*, 366.

(50). Chu, B.; Liu, X.; Li, X.; Zhang, Z.; Sun, J. Z.; Yang, Q.; Liu, B.; Zhang, H.; Zhang, C.; Zhang, X.-H. Phosphine-Capped Effects Enable Full-Color Clusteroluminescence in Nonconjugated Polyesters. *J Am Chem Soc*. **2024**, *146*, 10889-10898.

(51). Zhang, Z.; Xiong, Z.; Zhang, J.; Chu, B.; Liu, X.; Tu, W.; Wang, L.; Sun, J. Z.; Zhang, C.; Zhang, H.; Zhang, X.; Tang, B. Z. Near-Infrared Emission Beyond 900 nm from Stable Radicals in Nonconjugated Poly(diphenylmethane). *Angew. Chem. Int. Ed*. **2024**, *63*, e202403827.

(52). Lian, M.; Mu, Y.; Ye, Z.; Lu, Z.; Xiao, J.; Zhang, J.; Ji, S.; Zhang, H.; Huo, Y.; Tang, B. Z. Manipulating Noncovalent Conformational Lock via Side-Chain Engineering for Luminescence at Aggregate Level. *Aggregate*. **2024**, e560.

(53). Jim, C. K. W.; Qin, A.; Lam, J. W. Y.; Mahtab, F.; Yu, Y.; Tang, B. Z. Metal-Free Alkyne Polyhydrothiolation: Synthesis of Functional Poly(vinylenesulfide)s with High Stereoregularity by Regioselective Thioclick Polymerization. *Adv. Funct. Mater*. **2010**, *20*, 1319-1328.

(54). Wei, Q.; Pötzsch, R.; Liu, X.; Komber, H.; Kiriy, A.; Voit, B.; Will, P. A.; Lenk, S.; Reineke, S. Hyperbranched Polymers with High Transparency and Inherent High Refractive Index for Application in Organic Light-Emitting Diodes. *Adv. Funct. Mater*. **2016**, *26*, 2545-2553.

(55). Chen, J.; Dong, Z.; Li, M.; Li, X.; Chen, K.; Yin, P. Ultra-Strong and Proton Conductive

Aqua-Based Adhesives from Facile Blending of Polyvinyl Alcohol and Tungsten Oxide Clusters. *Adv. Funct. Mater*. **2022**, *32*, 2111892.

(56). Rahman, M. A.; Bowland, C.; Ge, S.; Acharya, S. R.; Kim, S.; Cooper, V. R.; Chen, X. C.; Irle, S.; Sokolov, A. P.; Savara, A.; Saito, T. Design of Tough Adhesive from Commodity Thermoplastics through Dynamic Crosslinking. *Sci. Adv*. **2021**, *7*, eabk2451.

(57). Zhao, Z. H.; Zhao, P. C.; Zhao, Y.; Zuo, J. L.; Li, C. H. An Underwater Long-Term Strong Adhesive Based on Boronic Esters with Enhanced Hydrolytic Stability. *Adv. Funct. Mater*. **2022**, *32*, 2201959.

(58). Cui, C.; Chen, X.; Ma, L.; Zhong, Q.; Li, Z.; Mariappan, A.; Zhang, Q.; Cheng, Y.; He, G.; Chen, X.; Dong, Z.; An, L.; Zhang, Y. Polythiourethane Covalent Adaptable Networks for Strong and Reworkable Adhesives and Fully Recyclable Carbon Fiber-Reinforced Composites. *ACS Appl. Mater. Interfaces*. **2020**, *12*, 47975-47983.

(59). Chen, S.-W.; Lu, P.; Zhao, Z.-Y.; Deng, C.; Wang, Y.-Z. Recyclable Strong and Tough Polyamide Adhesives via Noncovalent Interactions Combined with Energy-Dissipating Soft Segments. *Chemical Engineering Journal*. **2022**, *446*, 137304.

(60). Yang, J.; Zhou, X.; Yang, J.; Chen, J.; Sun, Z.; Cheng, Y.; Yang, L.; Wang, H.; Zhang, G.; Fu, J.; Jiang, W. A Microscale Regulation Strategy for Strong, Tough, and Efficiently Self-Healing Energetic Adhesives. *Chemical Engineering Journal*. **2023**, *451*, 138810.

(61). Wang, S.; Liu, Z.; Zhang, L.; Guo, Y.; Song, J.; Lou, J.; Guan, Q.; He, C.; You, Z. Strong, Detachable, and Self-Healing Dynamic Crosslinked Hot Melt Polyurethane Adhesive. *Mater. Chem. Front*. **2019**, *3*, 1833-1839.

(62). Sun, P.; Mei, S.; Xu, J. F.; Zhang, X. A Bio-Based Supramolecular Adhesive: Ultra-High Adhesion Strengths at both Ambient and Cryogenic Temperatures and Excellent Multi-Reusability. *Adv. Sci*. **2022**, *9*, 2203182.

(63). Sun, P.; Li, Y.; Qin, B.; Xu, J.-F.; Zhang, X. Super Strong and Multi-Reusable Supramolecular Epoxy Hot Melt Adhesives. *ACS Materials Lett*. **2021**, *3*, 1003-1009.

(64). Yao, Y.; Xu, Z.; Liu, B.; Xiao, M.; Yang, J.; Liu, W. Multiple H-Bonding Chain Extender-

Based Ultrastiff Thermoplastic Polyurethanes with Autonomous Self-Healability, Solvent-Free Adhesiveness, and AIE Fluorescence. *Adv. Funct. Mater*. **2020**, *31*, 2006944.

(65). Li, C.; Dong, W.; Li, L.; Dou, Z.; Li, Y.; Wei, L.; Zhang, Q.; Fu, Q.; Wu, K. A Strain-Reinforcing Elastomer Adhesive with Superior Adhesive Strength and Toughness. *Mater. Horiz*. **2023**, *10*, 4183-4191.

(66). Sun, J.; Xiao, L.; Li, B.; Zhao, K.; Wang, Z.; Zhou, Y.; Ma, C.; Li, J.; Zhang, H.; Herrmann, A.; Liu, K. Genetically Engineered Polypeptide Adhesive Coacervates for Surgical Applications. *Angew. Chem. Int. Ed*. **2021**, *60*, 23687-23694.